Fluxes and distribution of dissolved iron in the eastern (sub-) tropical North Atlantic Ocean

Micha J. A. Rijkenberg,[1,2] Sebastian Steigenberger,[1] Claire F. Powell,[3] Hans van Haren,[2] Matthew D. Patey,[1] Alex R. Baker,[3] and Eric P. Achterberg[1]

Received 6 December 2011; revised 16 May 2012; accepted 10 June 2012; published 21 July 2012.

[1] Aeolian dust transport from the Saharan/Sahel desert regions is considered the dominant external input of iron (Fe) to the surface waters of the eastern (sub-) tropical North Atlantic Ocean. To test this hypothesis, we investigated the sources of dissolved Fe (DFe) and quantified DFe fluxes to the surface ocean in this region. In winter 2008, surface water DFe concentrations varied between <0.1 nM and 0.37 nM, with an average of 0.13 ± 0.07 nM DFe (n = 194). A strong correlation between mixed layer averaged concentrations of dissolved aluminum (DAl), a proxy for dust input, and DFe indicated dust as a source of DFe to the surface ocean. The importance of Aeolian nutrient input was further confirmed by an increase of 0.1 nM DFe and 0.05 μM phosphate during a repeat transect before and after a dust event. An exponential decrease of DFe with increasing distance from the African continent, suggested that continental shelf waters were a source of DFe to the northern part of our study area. Relatively high Fe:C ratios of up to 3×10^{-5} (C derived from apparent oxygen utilization (AOU)) indicated an external source of Fe to these African continental shelf waters. Below the wind mixed layer along 12°N, enhanced DFe concentrations (>1.5 nM) correlated positively with apparent oxygen utilization (AOU) and showed the importance of organic matter remineralization as an DFe source. As a consequence, vertical diffusive mixing formed an important Fe flux to the surface ocean in this region, even surpassing that of a major dust event.

Citation: Rijkenberg, M. J. A., S. Steigenberger, C. F. Powell, H. van Haren, M. D. Patey, A. R. Baker, and E. P. Achterberg (2012), Fluxes and distribution of dissolved iron in the eastern (sub-) tropical North Atlantic Ocean, *Global Biogeochem. Cycles*, *26*, GB3004, doi:10.1029/2011GB004264.

1. Introduction

[2] Iron (Fe) is a key element for marine phytoplankton and, due to its low concentrations, controls primary productivity and dinitrogen fixation in large parts of the world's oceans [*de Baar et al.*, 1990; *Martin and Fitzwater*, 1988; *Moore et al.*, 2009]. In general, dissolved Fe (DFe) concentrations in surface oceans are very low as a consequence of the low solubility of the thermodynamically favored Fe(III) redox state [*Liu and Millero*, 2002]. Due to its low solubility, Fe(III) in seawater either rapidly forms colloidal and particulate phases or is scavenged by these phases [*Wu and Luther*, 1994]. However, organic complexation enhances the solubility of Fe over its inorganic solubility of 0.08–0.2 nM at 20°C [*Kuma et al.*, 1996; *Liu and Millero*, 2002]. With more than 99% of DFe in seawater being organically complexed, the concentration of ligands often exceeds the DFe concentration [*Gledhill and van den Berg*, 1994]. As a result, organic Fe-binding ligands determine the DFe distribution in dust impacted surface waters by facilitating the dissolution and stabilization of aerosol derived Fe [*Rijkenberg et al.*, 2008b; *Wagener et al.*, 2008]. In addition, the organic complexation of Fe influences its availability for biological uptake [*Hassler and Schoemann*, 2009; *Maldonado et al.*, 2005; *Rijkenberg et al.*, 2008a].

[3] Aeolian dust transport forms an important supply route of Fe to remote open ocean environments [*Jickells et al.*, 2005]. The North Atlantic Ocean receives about 43% of the global oceanic dust inputs, and its main sources are the Saharan desert and the Sahel region [*Duce et al.*, 1991; *Jickells et al.*, 2005]. Maximum dust deposition in the (sub-) tropical Northeast Atlantic Ocean occurs in winter when the Inter Tropical Convergence Zone (ITCZ) is located south of 5°N and dust is transported in the lower air masses by the northeasterly trade winds [*Chiapello et al.*, 1995]. Inputs of aerosol derived DFe not only depend on Aeolian supply but also on the dissolution of Fe which is determined by aerosol source/mineralogy, atmospheric (photo-) chemical processing,

[1]School of Ocean and Earth Science, National Oceanography Centre Southampton, University of Southampton, Southampton, UK.
[2]Royal Netherlands Institute for Sea Research, Den Burg, Netherlands.
[3]Laboratory for Global Marine and Atmospheric Chemistry, School of Environmental Sciences, University of East Anglia, Norwich, UK.

Corresponding author: M. J. A. Rijkenberg, Royal Netherlands Institute for Sea Research, Den Burg NL-1790 AB, Netherlands. (micha.rijkenberg@nioz.nl)

0886-6236/12/2011GB004264

aerosol size, conditions in the receiving seawater including ambient DFe concentration and dissolved organic Fe-binding ligand characteristics, dust loading (e.g., influencing scavenging), and the influence of biology on the aerosol particles following deposition [*Baker and Croot*, 2010].

[4] Continental shelves form another important source of DFe to the open ocean [*Johnson et al.*, 1997]. *Ussher et al.* [2010] observed a negative relationship between surface DFe concentrations and distance from the North West African coast, illustrating the role of the continental shelf as a source of DFe to the Canary Basin. Oxidation of organic material in the shelf sediments may lead to suboxic or anoxic conditions with reductive Fe-oxyhydroxide dissolution and subsequent release of DFe to the overlying water column [*Elrod et al.*, 2004]. In addition, upwelling of deep waters enhanced in DFe or release of Fe from upwelled biogenic and lithogenic particles along the North West African coast [*Neuer et al.*, 2002] may explain the gradient of surface DFe concentration with distance from the African continent. Horizontal transport of dissolved and particulate iron derived from continental shelf regions determined DFe distributions off the Californian coast [*Johnson et al.*, 1997], in the subarctic North Pacific [*Lam et al.*, 2006; *Nishioka et al.*, 2007], in the vicinity of the Crozet and Kerguelen Islands [*Blain et al.*, 2008; *Planquette et al.*, 2007] and in the polynyas of Pine Island Bay and the Amundsen Sea in the Southern Ocean [*Gerringa et al.*, 2012].

[5] A pronounced oxygen minimum zone (OMZ) is positioned south of the North Equatorial Current (NEC) and north of the North Equatorial Countercurrent (NECC) in the North Atlantic Ocean. The oxygen minimum is strongest at a depth of 400 to 500 m immediately above the boundary between the Central Water and Antarctic Intermediate Water (AAIW) [*Stramma et al.*, 2008]. Oxygen minimum zones are the result of a weak ocean ventilation preventing the supply of atmospheric oxygen, combined with enhanced organic matter respiration which consumes oxygen, in often highly productive oceanic regions [*Karstensen et al.*, 2008]. Dissolved Fe released due to organic matter remineralization is stabilized in solution by simultaneously released Fe-binding ligands, allowing for enhanced DFe concentrations in OMZs [*Boyd et al.*, 2010; *Hopkinson and Barbeau*, 2007; *Witter et al.*, 2000]. Furthermore, the low redox potential in OMZs may prevent oxidation of highly soluble Fe(II), as evidenced by relatively high Fe(II) concentrations in OMZs [*Hopkinson and Barbeau*, 2007; *Santana-Casiano et al.*, 2005].

[6] In recent years, the tropical North Atlantic Ocean has become a focus for research on the biogeochemical effects of Saharan dust inputs [*Dall'Osto et al.*, 2010; *Hill et al.*, 2010; *Rijkenberg et al.*, 2008b; *Ye et al.*, 2009]. Quantification of the various sources of DFe to the surface ocean is required to establish the relative importance of Aeolian Fe inputs. This study presents the distribution of DFe and the quantification of its various sources to the surface ocean of the eastern (sub-) tropical North Atlantic Ocean.

2. Materials and Methods

2.1. Sampling

[7] During a cruise in the tropical and subtropical Northeast Atlantic Ocean (5 January to 5 February 2008) on board the research vessel RRS *Discovery* (cruise D326), near-surface seawater was pumped into a trace metal clean laboratory container using a Teflon diaphragm pump (Almatec A-15, Germany) connected by an acid-washed braided PVC tubing to a towed fish positioned at approximately 3 m depth alongside the ship. Samples for DFe, dissolved aluminum (DAl), and nanomolar phosphate and nitrate were filtered in-line using a filter capsule (Sartorius, Sartobran 300) with a 0.2 μm filtration cut-off, and stored in acid-cleaned low-density polyethylene bottles (250 mL, Nalgene) [*Achterberg et al.*, 2001].

[8] Water column samples were collected with a trace-metal clean titanium CTD rosette system using 10-L Ocean Test Equipment (OTE) bottles modified for trace metal sampling. CTDs were in general deployed to 300 m, however, at 4 stations to 1800 m and at 2 stations to near the seafloor. Samples were processed on board in the trace metal clean laboratory container. The OTE bottles were pressurized with filtered high-purity nitrogen gas (BOC Gases), and seawater samples were directly filtered using a filter capsule (Sartorius, Sartobran 300) with a 0.2 μm filtration cut-off. Samples for DFe and DAl were acidified to pH 1.9 by addition of 1 mL of 12M HCl (Romil UHPgrade) per 1 L of sample.

[9] Oxygen was determined using a Seabird SBE 43 oxygen sensor on the CTD frame, calibrated using Winkler titrations on discretely collected samples from the CTD rosette. Underway seawater temperature and salinity were determined using the ship's thermosalinograph. Underway and CTD salinity measurements were calibrated using discretely collected salinity samples, analyzed at sea using a salinometer (Autosal, Guildline).

2.2. Nutrients, Trace Metals and Environmental Data

[10] Shipboard measurement of DFe (<0.2 μm) was performed by flow injection analysis with in-line preconcentration on a column of immobilized 8-hydroxyquinoline (8-HQ) [*Landing et al.*, 1986] and detection by chemiluminescence [*de Jong et al.*, 1998; *Obata et al.*, 1993]. At least half an hour prior to analysis, hydrogen peroxide (Romil SpA) was added to the samples (40 μL 0.03% H_2O_2 (v/v) stock solution to 40 mL sample) to oxidize any Fe(II) present. Samples were buffered in-line by addition of 2 M trace metal clean ammonium acetate buffer (Romil UHP ammonia and Romil SpA acetic acid) to obtain a final pH of ~4.0. Dissolved Fe was eluted from the column with 0.3 M HCl (Romil SpA). Chemiluminescence was induced by mixing the eluent with a 0.5 M hydrogen peroxide (Romil SpA) solution, a 0.8 M ammonia (Romil SpA) solution and last with the luminol solution consisting of 0.3 mM luminol (Sigma, used as received), 0.38 mM sodium carbonate (Sigma, grade SigmaUltra) and 0.7 mM triethylenetetramine (Sigma). All solutions were prepared using 18.2 MΩ cm de-ionized water (MQ, Millipore).

[11] The analytical blank was on average 0.042 ± 0.018 nM DFe (n = 31) and the average detection limit (3σ of the blank) was 0.022 ± 0.017 nM DFe. An average concentration of 0.60 ± 0.06 nM DFe (n = 7) was obtained for an Fe reference material from the IRONAGES intercomparison exercise (bottle 91), while the reported intercomparison value was 0.59 ± 0.21 nM DFe [*Bowie et al.*, 2006]. Analysis of SAFE reference samples for surface waters gave 0.084 ± 0.007 nM and 0.086 ± 0.005 nM DFe for SAFE-148s and

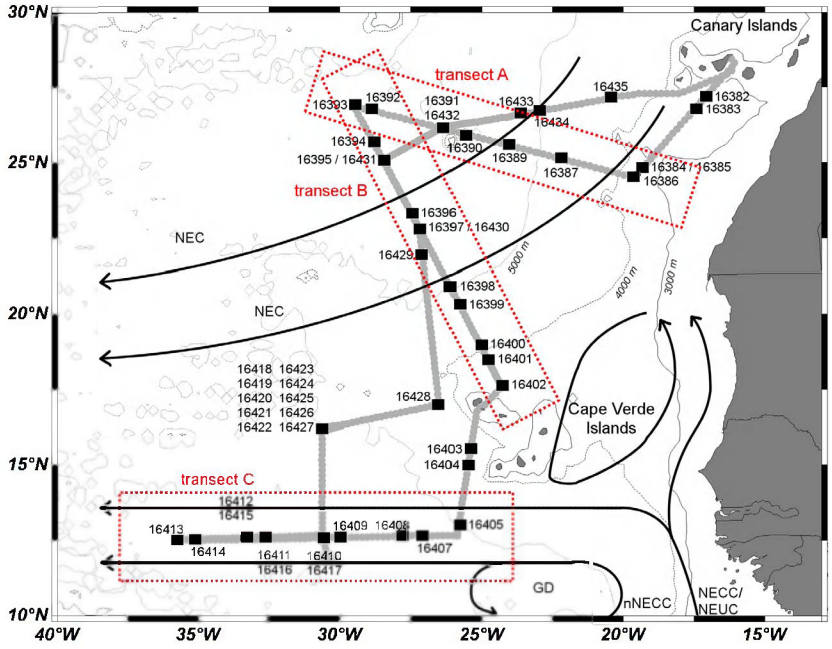

Figure 1. Map of the study area with the cruise track (gray) of the RRS *Discovery* sailed in January/February 2008. A total of 43 stations have been sampled. Most stations were sampled down to 300 m. St16395, st16412, st16416 and st16434 were sampled down to 1800 m, st16402 and st16435 were sampled down to 3650 and 4612 m, respectively. Stations are shown (black squares) together with station numbers and the large scale near-surface flow field depicted by black arrows [*Stramma et al.*, 2005, 2008]. Also indicated are the North Equatorial Current (NEC), the return flow of the northern North Equatorial Countercurrent (nNECC), the north flowing part of the North Equatorial Countercurrent (NECC) which is connected to the North Equatorial Undercurrent (NEUC), as well as the upwelling region named the Guinea Dome (GD). Transects A, B and C are marked in red.

SAFE-165s, respectively, and 0.92 ± 0.01 nM and 0.95 ± 0.02 nM DFe for the deep samples SAFE-336d and SAFE-458d, respectively. Reported consensus concentrations of the SAFE surface and deep samples are 0.097 ± 0.043 nM and 0.91 ± 0.17 nM DFe, respectively (http://www.geotraces.org/science/intercalibration).

[12] Dissolved Al was determined using a flow-injection fluorescence method with lumogallion as the fluorescent reagent [*Brown and Bruland*, 2008]. Apparent oxygen utilization (AOU) was calculated by subtracting the measured oxygen content from the oxygen saturation value [*Fofonoff and Millard*, 1983]. Phosphate was determined colorimetrically using the molybdenum blue method achieving a detection limit of 0.8 nM [*Patey et al.*, 2008]. Silicate was measured on a Skalar Sanplus segmented-flow autoanalyzer according to *Kirkwood* [1996].

2.3. Aerosol Sampling and Analysis

[13] Aerosols were collected on the RRS *Discovery* using a high volume (1 m^3 min^{-1}) aerosol sampler equipped with a Sierra-type cascade impactor for separation of particles into coarse (>1 μm diameter) and fine (<1 μm diameter) fractions. The soluble Fe and Al fraction of these samples were determined in a land-based laboratory by an ammonium acetate leach (pH 4.7, 1–2 h). The sampling and analysis methods employed have previously been described in detail [*Baker et al.*, 2006; *Sarthou et al.*, 2003]. Deposition velocities were based on a model by *Ganzeveld et al.* [1998] that takes into account the particle mass median diameter (MMD), wind speed, and values for the overall oceanic mean humidity and whitecapping [*Ganzeveld et al.*, 1998]. MMDs of 0.6 μm, for the fine fraction, and 5 μm, for the coarse fraction, were used based on data obtained from a Saharan dust aerosol sample that was segregated into 7 different size fractions during cruise ANT18-I [*Sarthou et al.*, 2003], according to the method of *Arimoto and Duce* [1986]. Details of this procedure can be found in *Powell* [2011].

2.4. Vertical Eddy Diffusivity Determinations Using CTD Data

[14] The Thorpe scale, a vertical length scale of turbulent mixing in a stratified flow [*Thorpe*, 1977], was used to calculate the vertical turbulent eddy diffusivity (K_z) from 0.5 m binned CTD data. Rearrangement of an observed potential density profile, which may contain inversions associated with turbulent overturns, into a stable profile without inversions provided the vertical displacement necessary for generating a stable profile and is defined as the Thorpe displacement. Occasional T-S loopings due to sensor mismatch of the temperature-conductivity sensor were removed [*Galbraith and Kelley*, 1996]. With d_T as the root mean square of the Thorpe displacements within each overturn, the eddy diffusivity (m^2 s^{-1}) is defined as,

$$K_z = 0.128\, d_T^2 N \quad (1)$$

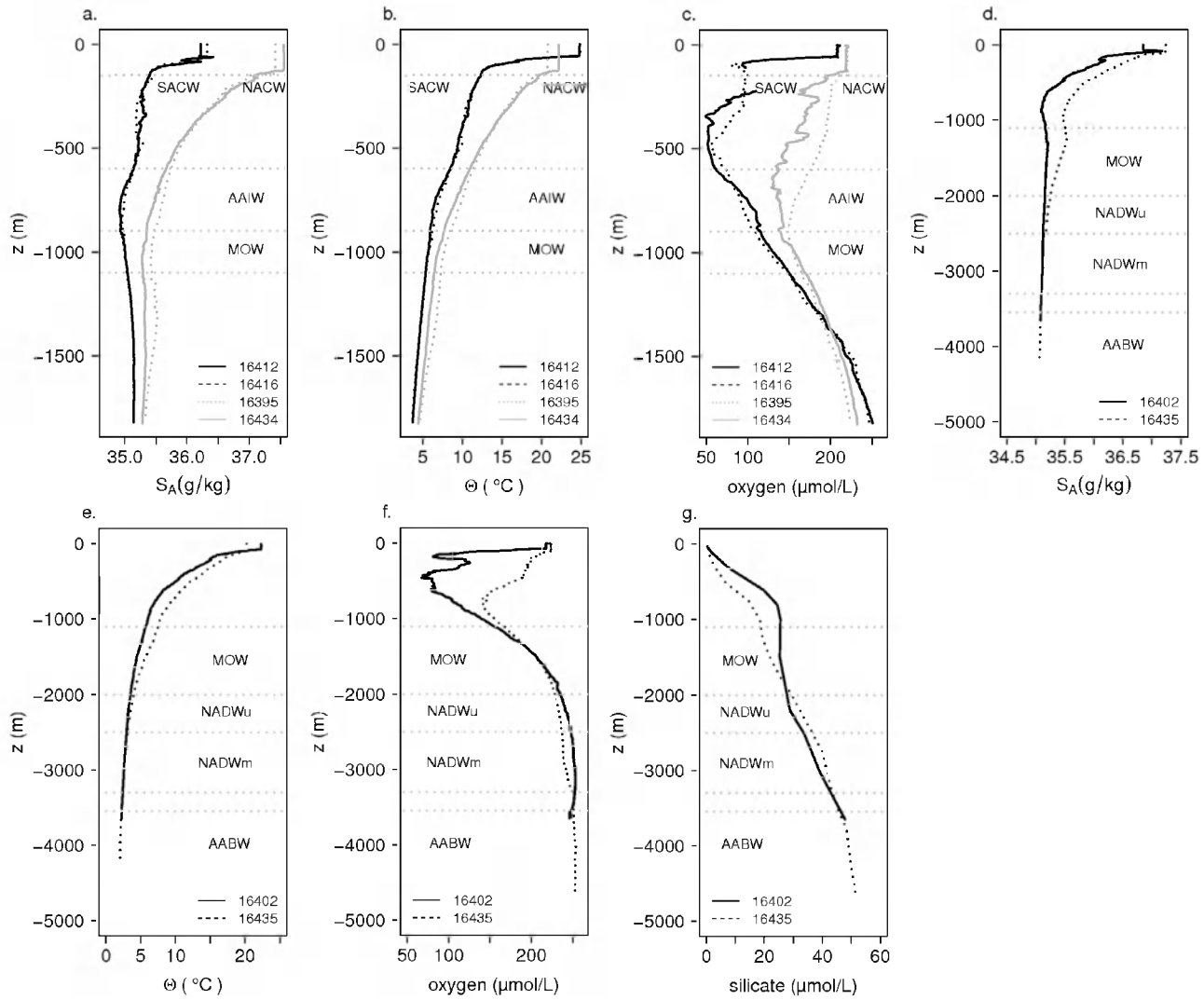

Figure 2. (a) Salinity (S_A), (b) conservative temperature (Θ) and (c) oxygen profiles for st16412 and st16416 at ~12.5°N, and st16395 and st16434 at ~25–27.5°N and (d) salinity (S_A), (e) conservative temperature (Θ), (f) oxygen and (g) silicate profiles for st16402 and st16435. Note that water mass designations are indicative only.

where N denotes the buoyancy frequency and the constant 0.128 follows from an empirical relation with the Ozmidov scale using a mixing efficiency of 0.2 [*Dillon*, 1982]. The method of overturn displacements provides an estimate of vertical turbulent eddy diffusivity and dissipation rate to within a factor of two compared with free-falling microstructure data [e.g., *Hosegood et al.*, 2005]. From the raw $K_z(z)$ profiles determined between the near-surface mixed layer depth (MLD) and MLD-50 m, a mean value was calculated and used to estimate fluxes for DFe.

3. Results and Discussion

3.1. Hydrography

[15] The study area is characterized by a complex current system in the upper 100 m of the water column [*Stramma and Schott*, 1999]. The Canary Current (CC) is a surface current flowing southward along the African coast between 30°N and 10°N, and is termed the North Equatorial Current (NEC) after diverting in a southwesterly direction (Figure 1) [*Stramma et al.*, 2005]. Surface currents south of the Cape Verde Islands comprise the northward and westward flowing parts of the North Equatorial Countercurrent (NECC) and the return flow of the northern North Equatorial Countercurrent (nNECC) [*Stramma et al.*, 2005]. At about 20°N, the Cape Verde Frontal Zone (CVFZ) corresponds with the boundary between the North Atlantic Central Water (NACW) and the South Atlantic Central Water (SACW).

[16] Figure 2 shows the salinity, temperature and oxygen profiles for the four stations sampled down to 1800 m. The salinity profiles show Tropical Surface Waters (TSW) with an enhanced salinity at depths between about 30 and 100 m for st16412 and st16416, and Antarctic Intermediate Water (AAIW) with a clear salinity minimum for st16412 and

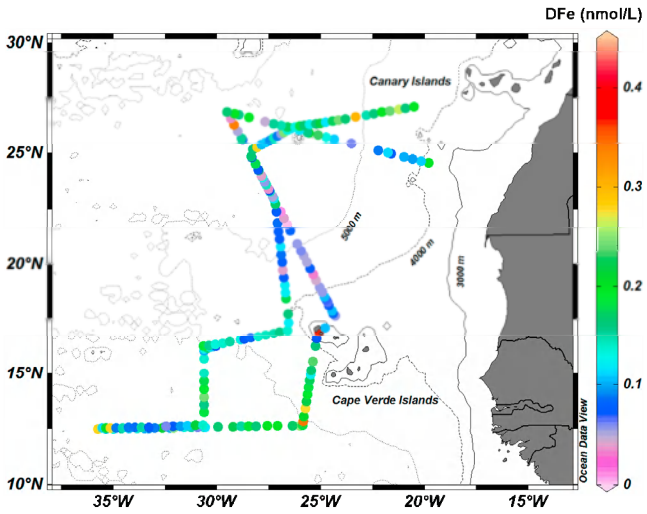

Figure 3. Contour map showing the near surface water DFe concentrations in nM during the RRS *Discovery* cruise in January/February 2008.

st16416 between ca. 600 and 900 m and becoming less distinct in northern parts of the study area (st16395 and st16434) due to mixing with relatively high salinity Mediterranean Outflow Waters (MOW) positioned between 1100–2000 m [*Machín and Pelegrí*, 2009; *Stramma et al.*, 2005; *Tsuchiya et al.*, 1992]. The temperature profiles show a sharp thermocline below the TSW for st16412 and st16416 in the SACW between 150 and 600 m with temperatures >8°C [*Stramma et al.*, 2005]. The NACW was positioned at similar depths for st16395 and st16343 to the north of the CVFZ [*Stramma et al.*, 2005]. The reduced rate of increase in silicate concentrations at ~2200 m for st16402 (Figure 2) indicated the upper North Atlantic Deep Water (NADWu) [*Tsuchiya et al.*, 1992]. The middle North Atlantic Deep Water (NADWm) at depths between ~2500 and 3300 m was characterized by an oxygen maximum for st16402 and by an intervening oxygen minimum at midlatitudes (between 18 and 30°N) for st16435 (Figure 2) [*Tsuchiya et al.*, 1992]. The increase in silicate concentrations below the NADWm for st16435 indicated dense cold water coming from the south and is often referred to as Antarctic Bottom Water (AABW) [*Tsuchiya et al.*, 1992].

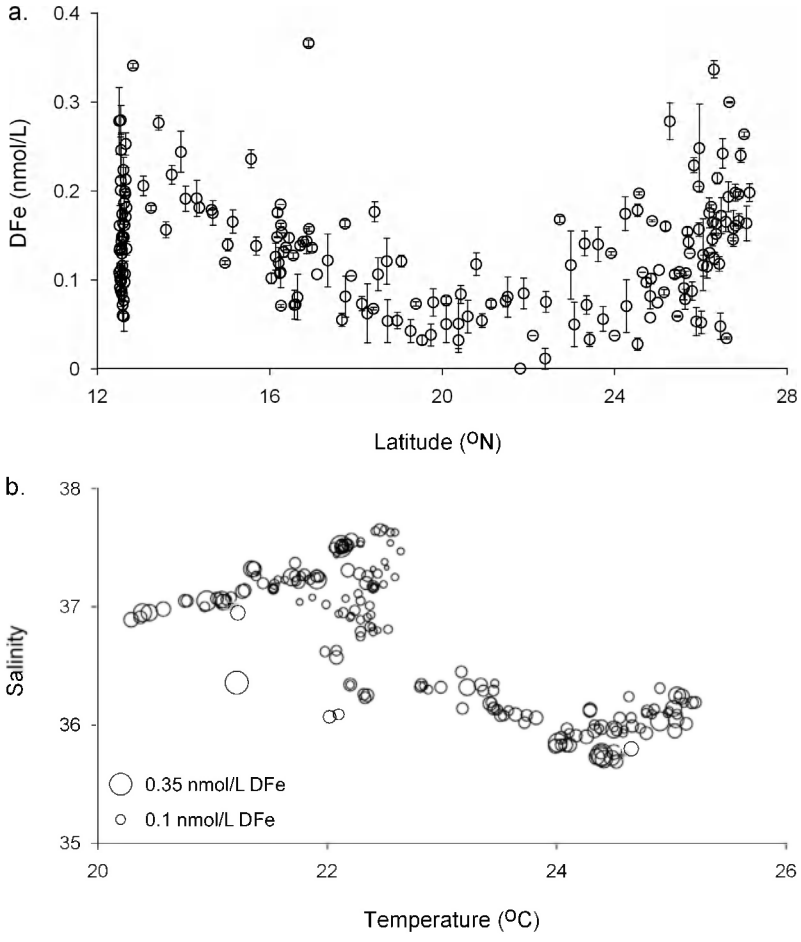

Figure 4. (a) The concentrations of surface water DFe (nM) plotted against latitude. Error bars represent the standard deviation (1σ). The large range in DFe concentrations at 12.5°N are the result of inclusion of DFe data from a longitudinal transect from ~25°W to ~35°W. (b) Bubble plot showing salinity against temperature (°C); bubble size is a relative representation of the DFe concentration.

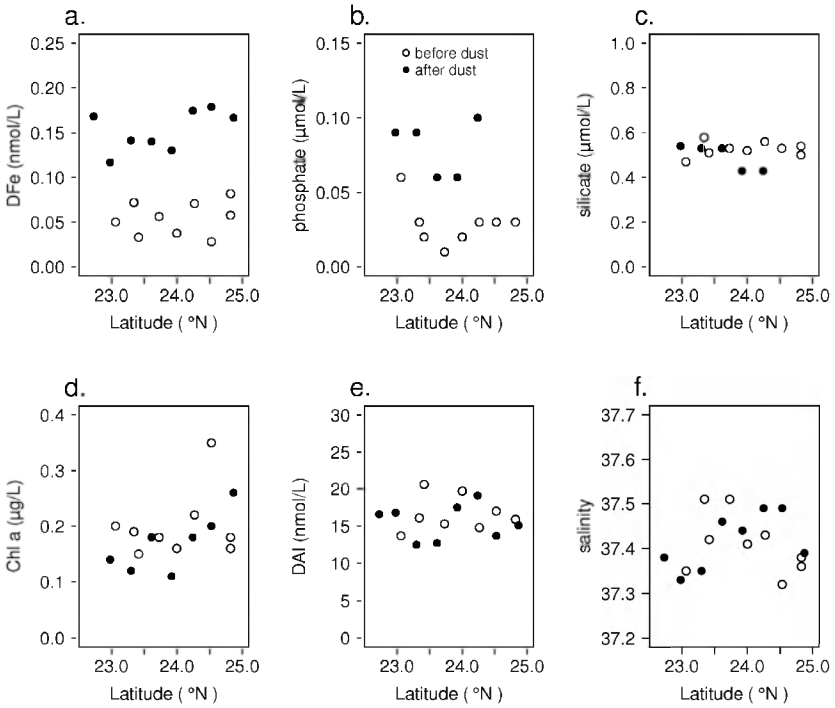

Figure 5. The surface water concentrations of DFe, phosphate, silicate, Chl a, DAI and salinity before and after a dust event between 25 and 30 January. The samples along the repeat transect were taken on 30 January, 5 days after the second dust event, and 18 days after the first transect was sailed (12 January).

3.2. Distribution of Surface Water Dissolved Fe

[17] The surface water DFe concentrations ranged between <0.1 nM and 0.37 nM, with an average of 0.13 ± 0.07 nM DFe (1σ, n = 194) (Figure 3). A similar range, with DFe concentrations between 0.1 and 0.4 nM, was observed in 2006 in the vicinity of the Cape Verde islands [*Rijkenberg et al.*, 2008b]. Furthermore, DFe concentrations were reported to range between ~0.2 and 0.55 nM along a meridional transect along ~19°W [*Sarthou et al.*, 2003]. In contrast to the distribution of surface DFe concentrations in 2006 [*Rijkenberg et al.*, 2008b], the DFe concentrations in this larger scale study of 2008 showed a clear latitudinal pattern (Figure 4a). The observed low DFe concentrations in 2008 coincided with a complex temperature-salinity pattern in the vicinity of the CVFZ (Figure 4b).

[18] In 2008, strong atmospheric dust events were encountered in the periods 17–19 January, and 25 January–01 February during occupation of st16405–st16409, and st16419–st16427, respectively (Figure 1). The second dust storm arrived from a northerly direction crossing over a transect between 22.5 and 25°N that we sailed for the first time 13 days earlier, and for a second time 5 days after the start of the dust event (25 January). This dust event resulted in a significant increase in surface DFe concentrations by 0.10 ± 0.04 nM, with concentrations of 0.05 ± 0.02 nM (n = 9) before and 0.15 ± 0.02 nM (n = 8) after the dust event (Student's t test, t-value = −9.56, df = 13.56, $p < 0.001$) (Figure 5). Also, the phosphate concentrations increased following the dust event from 0.03 ± 0.02 µM (n = 9) to 0.08 ± 0.02 µM (n = 8) (Student's t test, t-value = −5.37, df = 6.43, $p < 0.01$). Enhanced phosphate concentrations following dust events have been observed in the Mediterranean Sea [*Bartoli et al.*, 2005]. Furthermore, dust deposition models indicate that aerosols form an important source of phosphate to oligotrophic oceans [*Mahowald et al.*, 2008]. Concentrations of silicate, DAI, Chl *a* and salinity did not show statistically significant changes for the repeat transects, suggesting that no changes in water masses occurred in the 18 days between the repeat transect (Figure 5). A single dust event does not result in statistically significant increases in DAI as further explained below.

[19] Using the soluble Fe fraction of aerosols collected at sea in the period 25–30 January we calculated an increase of 0.032 ± 0.001 nM DFe for a 120 m mixed layer (Table 1). This value is somewhat lower than the observed increase of 0.10 ± 0.04 nM DFe in the surface waters (Figure 5). A similar good agreement between a measured increase in surface water DFe concentration and a calculated increase in DFe concentration using the soluble aerosol Fe fraction was reported by *Rijkenberg et al.* [2008b], after a dust event south of the Cape Verde Islands in 2006. Some of the difference between our calculated and observed DFe increases may be accounted for by some light rain shower activity around the ship on 26 January, increasing the atmospheric flux of dust and DFe to the sea surface. There was however insufficient rainfall in the vicinity of the ship to enable a measurable volume of rainwater to be collected. In addition, the presence of free Fe-binding ligands probably increased the solubility of aerosol Fe in seawater [*Rijkenberg et al.*, 2008b; *Wagener et al.*, 2008]. Furthermore, there are large uncertainties in deposition velocity estimates [*Duce et al.*, 1991]

Table 1. The Estimated Increase in Soluble Fe and Al Concentrations as a Result of Dust Inputs in the Period Between the Start of a Dust Event on 25 January 2008 and the Sailing of the Repeat-Transect on 30 January 2008 in the Region 22.5–25°N[a]

Start Date	Start Time (UTC)	Start Decimal Lat	Start Decimal Long	End Decimal Lat	End Decimal Long	Dep. Vel.[b] 0.6 μm (cm s^{-1})	Dep. Vel.[b] 5 μm (cm $s^{-1)}$	F_{Fe}[c] (mol m^{-2} s^{-1} $\times$ 10^{-11})	F_{Al}[c] (mol m^{-2} s^{-1} $\times$ 10^{-11})	Sample Period[d] (hrs)	D_{Fe} (mol m^{-2} $\times$ 10^{-7})	D_{Al} (mol m^{-2} $\times$ 10^{-6})
25/01/2008	13:08	16.19	−30.65	16.22	−30.66	0.021	0.47	0.32 ± 0.006	3.67 ± 0.026	18.37	2.14 ± 0.042	2.43 ± 0.017
26/01/2008	08:00	16.22	−30.66	16.21	−30.64	0.022	0.69	0.48 ± 0.013	4.56 ± 0.055	11.37	1.95 ± 0.052	1.87 ± 0.023
26/01/2008	19:00	16.21	−30.64	16.23	−30.65	0.022	0.72	0.53 ± 0.012	5.62 ± 0.052	11.38	2.18 ± 0.050	2.30 ± 0.021
27/01/2008	06:30	16.24	−30.65	16.56	−28.80	0.046	1.43	0.60 ± 0.012	5.93 ± 0.049	26.5	5.69 ± 0.113	5.65 ± 0.047
28/01/2008	09:00	16.59	−28.63	18.96	−26.73	0.052	1.55	1.38 ± 0.020	12.7 ± 0.062	26.63	13.3 ± 0.195	12.1 ± 0.060
29/01/2008	13:00	19.13	−26.75	22.64	−27.18	0.031	0.99	0.78 ± 0.011	8.01 ± 0.040	24.63	6.87 ±0.099	7.10 ± 0.037
30/01/2008	13:00	22.79	−27.20	25.25	−28.15	0.045	1.18	0.74 ± 0.011	7.62 ± 0.039	23.5	6.27 ± 0.089	3.15 ± 0.016
Time weighted average Fe and Al fluxes								0.75 ± 0.01	7.41 ± 0.05			
Total increase in soluble Fe and Al concentrations in nM[e]											0.032 ± 0.001	0.29 ± 0.002

[a]Start and finish time of each sample period are shown. F_{Fe} and F_{Al} are the dry deposition fluxes of soluble Fe and Al calculated from measured *atmospheric* concentrations, D_{Fe} and D_{Al} are the deposition amounts per unit area of soluble Fe and Al during each sample period. The calculation of the increase in soluble Fe and Al assumes no loss term for the atmospheric input of soluble Fe and Al. The average MLD of 120 m was used to calculate the increase in DFe and DAl concentrations.

[b]Deposition velocities were based on a model by *Ganzeveld et al.* [1998], see Section 2.3. Errors are propagated from uncertainties in the aerosol concentrations. Note that the much larger error in the deposition flux is not included in these error values.

[c]The reported soluble Fe and Al fluxes are the combined soluble Fe and Al from the fine dust as well as the coarse dust fraction. Time weighted average Fe and Al fluxes were calculated according to: Σ(flux x sample period) / total sample period.

[d]The time used to change the filter was included in the sample period. Half of the time necessary to exchange a filter was included with the previous sample period and half was included with the next sample period.

[e]The soluble Fe and Al concentration (nM) during each sample period was calculated (soluble Fe flux during sample period/(mixed layer depth × 1000)) and summed to get the total increase in the soluble Fe and Al concentration in nM for the period 25–30 January 2008.

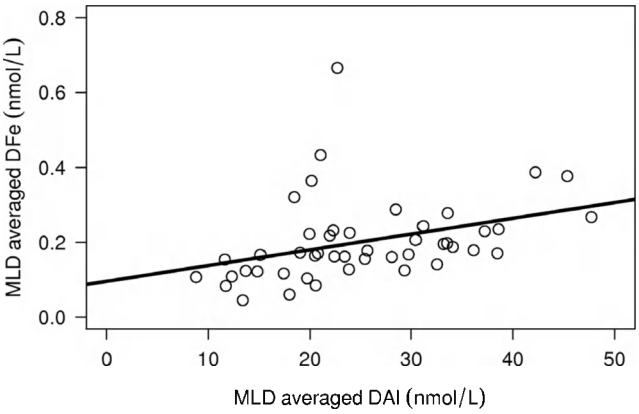

Figure 6. Linear regression shows a significant correlation ($p < 0.05$, $F_{1,44} = 6.45$, $R^2 = 0.13$) between mixed layer averaged DFe and DAl.

and the deposition of dust can be quite variable in space and time potentially resulting in differences between the measured and the calculated increase in DFe.

[20] Although DAl is often used as a proxy of dust input [*Measures and Vink*, 2000], the increase in DFe concentrations was not accompanied by a noticeable increase in DAl. An increase in DAl as a result of an individual dust event will remain unnoticed within the variation of measured DAl concentrations resulting from cumulative dust events [*Rijkenberg et al.*, 2008b]. For example, using the soluble Al fraction of aerosols collected by the high-volume aerosol collector for the period 25–30 January, we calculated an expected increase of 0.29 ± 0.002 nM DAl (1σ) for a 120 m mixed layer (Table 1). However, the DAl concentrations measured along this repeat transect were 16.6 ± 2.4 nM (1σ, n = 8) before and 15.5 ± 2.4 nM (1σ, n = 8) after the dust event. Thus the variation in the DAl concentrations in the surface waters was greater than the expected increase in DAl based on calculations using the soluble aerosol DAl fraction. Nevertheless, the cumulative effect of dust input resulted in a significant linear relationship between concentrations of DFe and DAl averaged over the MLD (Figure 6) confirming that dust input formed an important source of DFe to the surface ocean in our study region.

3.3. Distribution of Upper Ocean Dissolved Fe

[21] To investigate the distribution of DFe in the upper ocean, three transects were sailed to and from the African continent (Figure 7). Along the northernmost transect A (Figure 7a), the DFe concentrations in the upper 200 m decreased exponentially with increasing distance from the African continent ($R^2 = 0.67$, $p < 0.001$, DFe (nM) = $0.65e^{-x/576}$ with x the distance in km)). The decrease in DFe coincided with an increase in DAl along transect A, as also reported by *Ussher et al.* [2010] for a transect in the same region. Thus a continental source of waters rich in DFe but not DAl influenced the DFe distribution [*Sarthou et al.*, 2003]. The source of DFe may either be anoxic shelf sediments or the upwelling of deep waters rich in DFe along the continental shelf [*Elrod et al.*, 2004; *Neuer et al.*, 2002]. Our observation suggests that for this area the shelf formed the major source of DFe and not the input of dust. Because of the strong flow of the alongshore Canary Current (0.1–0.3 m s^{-1} [*Wooster et al.*, 1976]) perpendicular to the advective DFe transfer from the continental shelf, the source of DFe was most likely situated north of our transect A at 25°N.

[22] DFe concentrations, at depths between 100 and 300 m along transects B and C, correlated positively with the apparent oxygen utilization (AOU) (Transect B: $R^2 = 0.53$, $F_{1,33} = 35.53$, $P < 0.001$, 4 data points with Cook's distance > 0.5 removed; Transect C: $R^2 = 0.45$, $F_{1,28} = 22.82$, $P < 0.001$) (Figures 7b and 7c). As the AOU represents the oxygen used by heterotrophic bacteria during remineralization of organic matter, the good correlation between DFe and AOU suggests that this process formed a significant source of DFe at depths between 100 and 300 m in the vicinity of the Cape Verde islands. Remineralization as a source for DFe in the upper water column is further confirmed by the coinciding depths of the ferricline and nutricline for the large majority of stations.

[23] In our study area, the Fe:C ratio (C calculated using a ratio of AOU to C = 1.39 [*Anderson*, 1995]) for AOU observations between the MLD and 350 m was $4.78 \pm 3.29 \times 10^{-6}$ (1σ, n = 169) (Figure 8a). Our values were about half the Fe:C ratio of 1.1×10^{-5} reported for the North Atlantic oxygen minimum zone at 10°N using an AOU:C ratio of 1.6 [*Bergquist and Boyle*, 2006] and similar to Fe:C ratios found in the low Fe waters of the North Atlantic Ocean [*Boyd et al.*, 2007; *Sunda*, 1997]. Only in the northern part of our study area did high Fe:C ratios of up to $\sim 3.0 \times 10^{-5}$ reveal a clear external source of DFe (Figures 8a and 8c). These high values were similar to the average Fe:C ratio of 2.0×10^{-5} found to the north of our study area [*de Jong et al.*, 2007]. The high Fe:C ratios north of 20°N coincided with enhanced DFe concentrations originating from the continental shelf suggesting that the continental shelf forms an important source of external DFe in the northern part of our study region. Relatively lower Fe:C ratios with a mean of 4×10^{-6} were found at low oxygen concentrations south of 20°N (Figure 8b). There, the high DFe concentrations in the OMZ can therefore be attributed to remineralization of organic matter.

[24] A negative linear relationship between Fe:C ratios and oxygen concentration ($R^2 = 0.39$, $F_{1,100} = 62.89$, $P < 0.001$, Figure 8b) suggests that external sources of Fe, e.g., Aeolian Fe supply, increased the Fe:C ratio in the OMZ. Solubilization and stabilization of Fe from sinking dust particles by organic Fe-binding ligands released during organic matter remineralization may occur [*Hopkinson and Barbeau*, 2007; *Witter et al.*, 2000]. In addition, organic material enriched in Fe through luxury planktonic iron uptake in surface waters with enhanced Aeolian Fe inputs [*Bergquist and Boyle*, 2006; *Sunda*, 1997] yielded increasing Fe:C ratios with decreasing oxygen concentrations in the OMZ. Another reason could be that the Fe:C ratio of the organic material changed due to changes in the phytoplankton community. For example, a high abundance of the nitrogen fixer *Trichodesmium* spp., which has a relatively high Fe requirement [*Berman-Frank et al.*, 2001] and whose highest abundance is associated with enhanced surface water Fe concentrations from atmospheric inputs [*Moore et al.*, 2009;

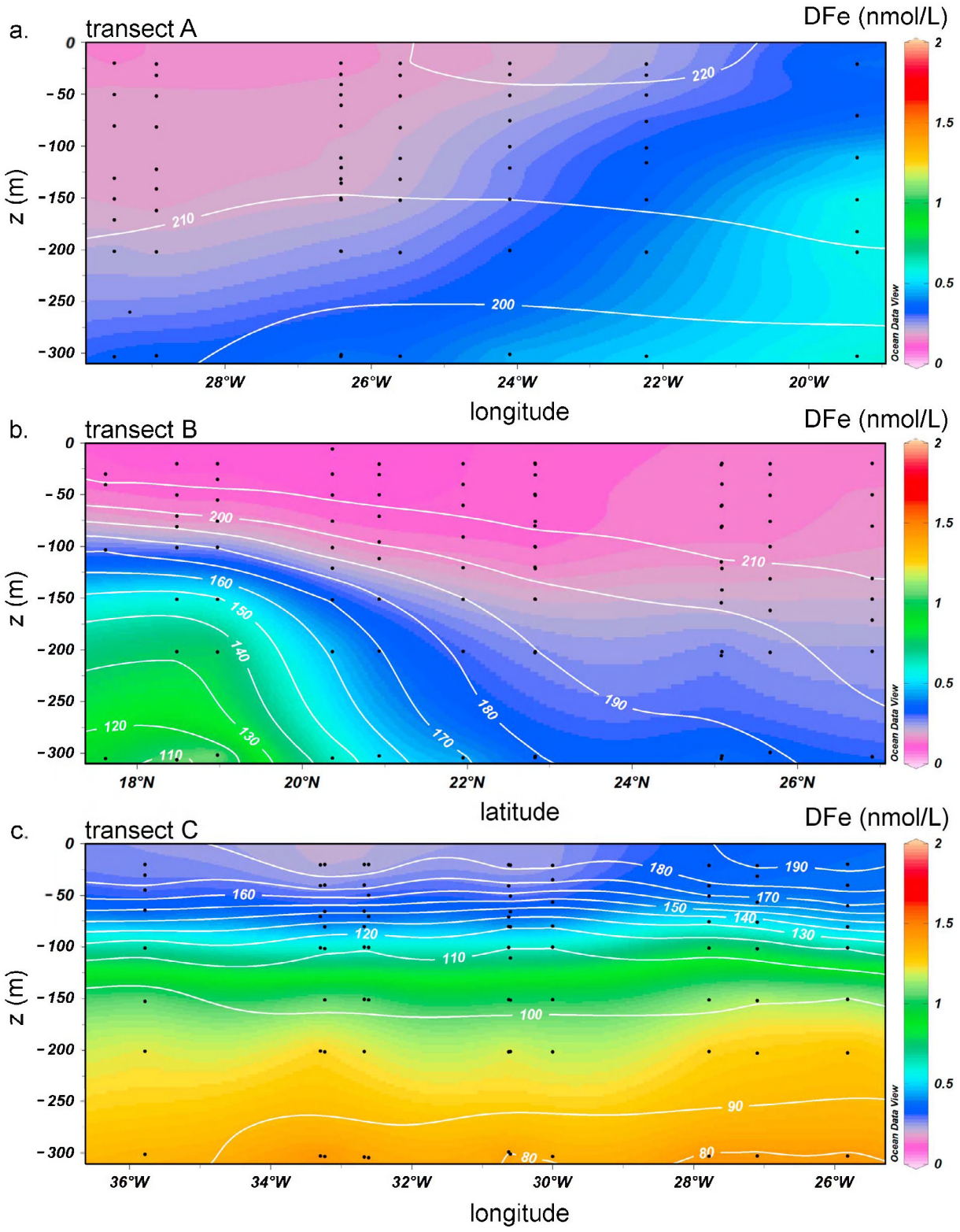

Figure 7. Section plots for DFe (nM) with oxygen (μmol/L) represented by white contour lines for (a) a section between st16386 and st16393 (transect A), (b) a section between st16393 and st16402 (transect B), and (c) a section between st16407 and st16413 (transect C).

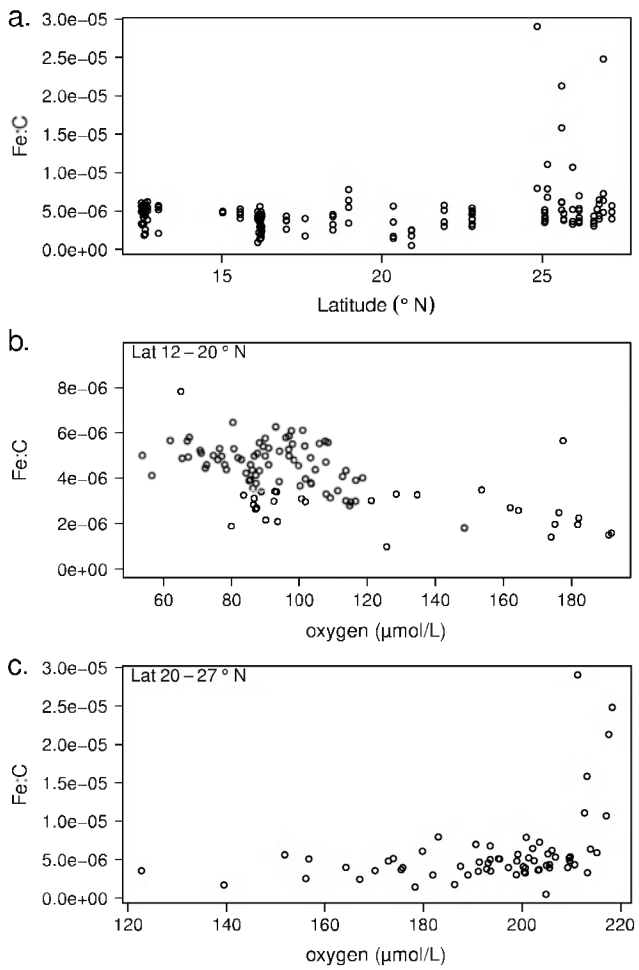

Figure 8. (a) Fe:C ratios for all data below the MLD and between 100 and 300 m as function of latitude, (b) Fe:C ratios as function of oxygen for latitudes 12–20°N, and (c) Fe:C ratios as function of oxygen for latitudes 20–27°N. Note the different scale in Figure 8b.

Rijkenberg et al., 2011], would result in higher Fe:C ratios at lower oxygen concentrations in the OMZ.

3.4. Deep Water Dissolved Iron Concentrations

[25] Deep water DFe concentrations have been determined at six stations. St16412 and st16416 were situated at the main core of the OMZ to the southwest of the Cape Verde islands along ~12.5°N and three stations, st16395, st16434 and st16435, to the north and northeast of the Cape Verde Islands between ~25 and 27.5°N (Figure 9). Station 16402, at the Tropical Eastern North Atlantic Time series Observatory (TENATSO) site north of the Cape Verde islands, will be described separately.

[26] The OMZ was situated between 300 and 1200 m (Figure 2c). As a consequence, variability in DFe concentrations between the different water masses present at these depths was the result of variability in the magnitude of organic matter remineralization. This is confirmed by the close correlation between DFe and AOU in the NACW and SACW ($R^2 = 0.93$, $F_{1,12} = 150.6$, $p < 0.001$), and the high mean concentration of DFe (1.45 ± 0.16 nM, 1σ, n = 2) in the AAIW within the OMZ as compared to lower DFe concentrations of 0.72 ± 0.10 nM (1σ, n = 7) in the AAIW north and northeast of the Cape Verde islands. DFe concentrations in the OMZs of the eastern subtropical North Pacific Ocean and the Arabian Sea were up to 1.2 and between 1.2 and 2.6 nM, respectively [*Hopkinson and Barbeau*, 2007; *Witter et al.*, 2000], compared to 1.2–1.85 nM DFe at ~33°W to the southwest of the Cape Verde Islands. To the east of stations st16412 and st16416, at 29°W, DFe concentrations of up to 2 nM were reported within the OMZ at 400 m depth [*Measures et al.*, 2008]. In contrast with our study, the DFe concentrations in the oxygenic waters immediately outside the OMZs in the eastern subtropical North Pacific Ocean and the Arabian Sea were similar to the concentrations within the OMZs suggesting sources other than remineralization determine the DFe concentrations including e.g., dust and benthic continental shelf supply [*Hopkinson and Barbeau*, 2007; *Landing and Bruland*, 1987; *Witter et al.*, 2000].

[27] The MOW, positioned between AAIW and NADW (between ~1100–1800 m), had a mean DFe concentration of 0.99 ± 0.11 nM (1σ, n = 4) for the region to the southwest of Cape Verdes and 0.62 ± 0.10 nM (1σ, n = 8) north to northeast of the Cape Verdes. The DFe concentration in the MOW northeast of the Cape Verdes is close to the DFe concentration of 0.74 ± 0.17 nM (1σ, n = 2) as reported for MOW in the Bay of Biscay [*Laës et al.*, 2003] and the DFe concentration of 0.57 nM as reported for MOW at 39°44′N, 14°10′W [*Thuróczy et al.*, 2010]. Most likely, the DFe concentration in the MOW increases while flowing southwards due to Fe supply through remineralization of sinking organic matter.

[28] Full depth profiles were sampled at st16435 west of the Canary Islands and st16402 at the TENATSO site. With the exception of surface water concentrations, the DFe concentrations for st16402 situated directly under the Saharan dust plume were higher than those observed for st16435. The strong correlation between AOU and DFe shows that the DFe concentrations at depths between 300 and 1200 m for st16402 and 16435 were also primarily determined by the mineralization of organic matter. The DFe concentrations in the NADW between 1800 m and 3500 m decreased slightly with depth for both stations with mean DFe concentrations of 0.48 ± 0.05 nM (1σ, n = 5) for st16435 and 0.80 ± 0.08 nM (1σ, n = 3) for st16402. The DFe concentrations in the NADW for st16435 were similar to the DFe concentrations ranging between 0.39 and 0.54 nM reported for the NADW north of the Canary Islands [*de Baar et al.*, 2008; *Sarthou et al.*, 2007]. The enhanced DFe concentrations in the NADW at st16402 compared well with DFe values of around 0.8 nM reported for the NADW at 10°N 45°W [*Bergquist and Boyle*, 2006]. Only st16435 was sufficiently deep to observe AABW, as indicated by relatively high silicate concentrations (>45 μM). The concentration of DFe in the AABW was lower (0.32 ± 0.02 nM; 1σ, n = 3) than in the overlying waters and consistent with the DFe concentrations <0.4 nM reported for AABW in the South Atlantic [*Klunder et al.*, 2011]. The DFe concentration just above the seafloor was 0.28 nM and slightly lower than the DFe in the AABW. Lower DFe concentrations within 50 m of the bottom have been observed by other workers and attributed to DFe scavenging by resuspended sediment particles.

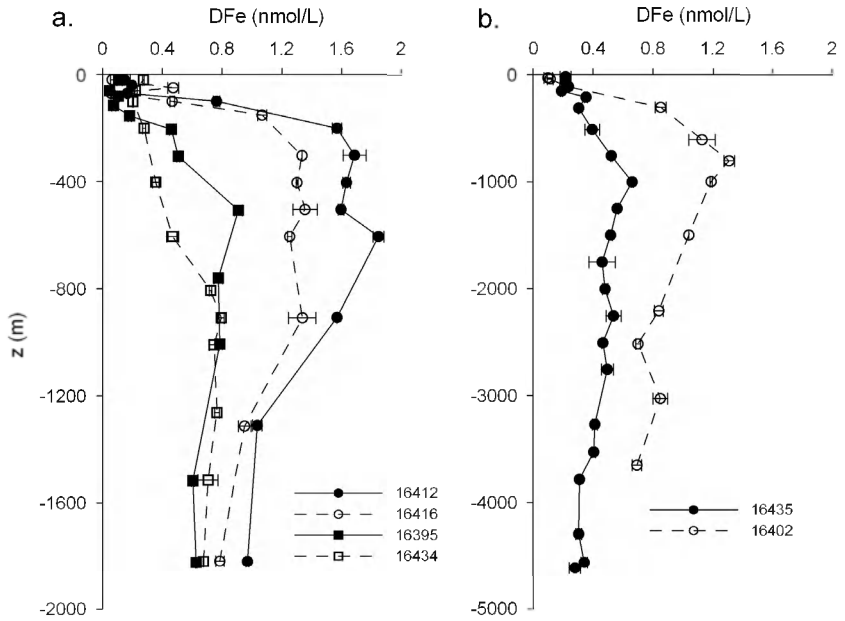

Figure 9. (a) DFe concentrations for st16412 and st16416 along ~12.5°N, and st16395 and st16434 at ~25–27.5°N, and (b) the DFe concentrations for st16402 (TENATSO site) and st16435 at ~27.5°N.

3.5. DFe Fluxes

[29] Calculated DFe fluxes were used to assess the importance of DFe supplies to the surface waters for an atmospheric dust event, continental shelf supply and vertical fluxes through the thermocline. A dust derived flux of 2.45×10^{-11} mol m^{-2} s^{-1} DFe was determined by using the average increase in DFe over a mean 120 m MLD after a dust event for a period of 134 h starting 25 January until 30 January when the RRS *Discovery* repeated the transect between 22.5 and 25°N. This flux-value was of the same order of magnitude as the average soluble Fe flux of $0.69 \pm 0.34 \times 10^{-11}$ mol m^{-2} s^{-1} calculated using the soluble Fe fraction of aerosols collected by the high-volume aerosol collector in the period between 25 and 30 January. Note that this dust derived flux of DFe is based on a single dust event and is consequently not representative of the yearly average dust derived DFe flux.

[30] The horizontal turbulent flux of DFe was calculated for two depth intervals along transect A: 0-MLD m and MLD-205 m. For the lateral turbulent flux calculation, the concentrations of DFe were fitted using the equation

$$C(x) = C_0 e^{-x/D} \quad (2)$$

where C_0 is the concentration at st16384, x is the distance (km) from st16384, and D is the scale length (km), defined as the distance over which concentrations of DFe decrease to 1/e of the initial value [*Johnson et al.*, 1997]. For the mixed layer, the exponential fit was [DFe] = $0.6464e^{-x/451}$ ($R^2 = 0.54$, $p < 0.001$) and for waters below the MLD the exponential fit was [DFe] = $0.6654e^{-x/582}$ ($R^2 = 0.79$, $p < 0.001$) (Figure 10). The excellent fit for the data displaying an exponential decrease of DFe with distance from the shore suggests a dominant role for eddy

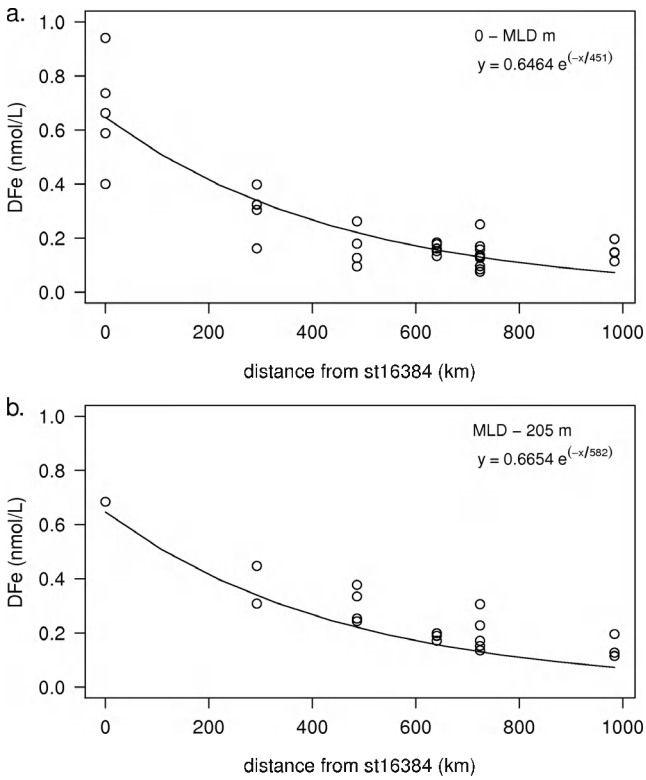

Figure 10. The DFe concentration in (a) the mixed layer and (b) between the MLD and 205 m for a transect between st16834 and st16393 (transect A). St16384 is closest to the African continental shelf and its x-position is set to 0 km.

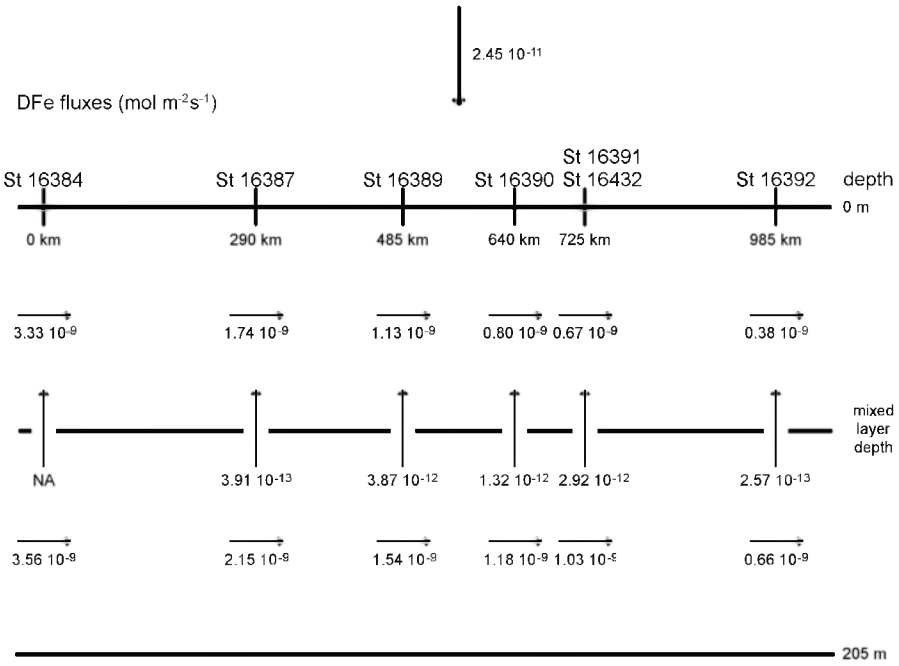

Figure 11. Schematic of the DFe fluxes originating from the African continental shelf, atmospheric dust inputs and vertical diffusion over the thermocline between st16384 and st16392 (transect A).

diffusive mixing as compared to onshore or offshore advective transport [*Moore*, 2000]. The value of 451 and 582 km obtained for D are large compared to most reported scale lengths. For example, reported values for D varied between 16 and 131 km for near surface DFe concentrations (0–100 m) in Monterey Bay, near the Crozet and Kerguelen Islands, the Antarctic Peninsula and in the Pine Island Polynya [*Ardelan et al.*, 2010; *Bucciarelli et al.*, 2001; *Gerringa et al.*, 2012; *Planquette et al.*, 2007]. However, Johnson *et al.* (1997) reported a scale length of 5000 km for DFe transport at 1000 m depth offshore of California.

[31] With the use of D, *Okubo*'s [1971] parameterization to estimate horizontal turbulent diffusivity (K_h, $m^2\ s^{-1}$) can be used:

$$K_h = 7.3 \times 10^{-4}\ D^{1.15}, \quad (3)$$

in which a 95% reduction length-scale l is used, $l = 3D$. The horizontal turbulent flux is then calculated as:

$$F = K_h \partial C/\partial x, \quad (4)$$

or

$$F(x) = -7.3 \times 10^{-4} D^{0.15} C(x). \quad (5)$$

Within the mixed layer, calculated DFe fluxes ranged from 3.33×10^{-9} mol $m^{-2}\ s^{-1}$ at st16384 to 0.38×10^{-9} mol $m^{-2}\ s^{-1}$ at st16392 (985 km further away from the African continental shelf). DFe fluxes below the MLD were similar and ranged from 3.56×10^{-9} mol $m^{-2}\ s^{-1}$ at st16384 to 0.66×10^{-9} mol $m^{-2}\ s^{-1}$ at st16392. Note that, because the dust derived DFe fluxes and the vertical DFe fluxes are between 2 and 4 orders of magnitude smaller than the lateral DFe flux, we did not correct the lateral DFe fluxes for the influence of these DFe fluxes.

[32] The vertical turbulent eddy diffusivity (K_z) determined over a depth range from MLD to MLD-50 m for stations of three transects (see Table S1 in the auxiliary material) had an overall mean value of $1.23 \pm 1.45 \times 10^{-3}\ m^2\ s^{-1}$ (1σ, n = 26) ranging between 0.048 and $6.5 \times 10^{-3}\ m^2\ s^{-1}$.[1] Our K_z values compared well with values between 0.3 and $0.8 \times 10^{-3}\ m^2\ s^{-1}$ as determined using the Thorpe scale method and reported by *Blain et al.* [2008] and *Gerringa et al.* [2012], over depth ranges between 100 and 300 m. Although, our values are higher than values of $0.01–0.07 \times 10^{-3}\ m^2\ s^{-1}$ determined using the diffusion of SF_6 gas during SOIREE and FeCycle in the first 100 m of the water column [*Boyd et al.*, 2005; *Law et al.*, 2003], they compare well with values ranging between 0.15 and $10 \times 10^{-3}\ m^2\ s^{-1}$ using a one dimensional model to describe the ^{228}Ra distribution over the thermocline in the upper 300 m on the Crozet plateau [*Charette et al.*, 2007]. The vertical turbulent DFe flux through the thermocline was calculated from the K_z and the DFe gradient ($\partial DFe/\partial z$, Table S1) according to,

$$F_{DFe} = K_z \partial DFe/\partial z. \quad (6)$$

The mean vertical turbulent DFe flux over the thermocline was $0.99 \pm 1.7 \times 10^{-11}$ mol $m^{-2}\ s^{-1}$ DFe (1σ, n = 26) with a range of $0.014–7.3 \times 10^{-11}$ mol $m^{-2}\ s^{-1}$ DFe. The highest vertical turbulent DFe fluxes occurred along the 12°N longitudinal section and coincided with the steepest gradients in DFe (corresponding with high AOU values).

[1] Auxiliary materials are available in the HTML. doi:10.1029/2011GB004264.

[33] Along transect A, three fluxes of DFe to the surface ocean could be distinguished including i) lateral diffusion from the continental shelf, ii) atmospheric dust deposition, and iii) vertical diffusion from below the thermocline. Figure 11 visualizes the fluxes and shows that lateral diffusion of DFe from the African continental shelf was the dominant flux of DFe along transect A. Assuming the same Aeolian flux of DFe (2.45×10^{-11} mol m^{-2} s^{-1}) for the whole study area during this dust event, dust was a more important source of DFe to the latitudinal transect along transect B than vertical diffusion (mean of $2.57 \pm 2.10 \times 10^{-12}$ mol m^{-2} s^{-1} (1σ, n = 10, range of 0.143–5.53 $\times$ 10^{-12} mol m^{-2} s^{-1}). However, along transect C the flux of Aeolian DFe was similar and at some places even lower than the vertical diffusion of DFe over the thermocline (mean of $2.19 \pm 2.36 \times 10^{-11}$ mol m^{-2} s^{-1} (1σ, n = 10, range of 0.322–7.3 $\times$ 10^{-11} mol m^{-2} s^{-1}). Although vertical fluxes of DFe from below the thermocline were similar to the Aeolian DFe flux it is noted that the DFe below the mixed layer may be the result of Aeolian DFe input over time either directly via the solubilization and stabilization of Fe from dust or with organic material settling from the surface ocean. Because transect B was a latitudinal transect we were unable to investigate a continental shelf derived lateral DFe flux. Furthermore, any potential lateral DFe flux originating from the continental shelf along the longitudinal transect C was too small to result in a measurable gradient in DFe and as a consequence was not further considered here. An extension of transect C along 12°N in the direction of the continental shelf would allow us to calculate a lateral DFe flux for this region.

4. Conclusion

[34] Some of the highest N_2 fixation rates and diazotroph abundances have been reported for the heavily dust impacted eastern (sub-) tropical North Atlantic Ocean [*Langlois et al.*, 2008; *Voss et al.*, 2004] and especially south of the Cape Verde islands [*Rijkenberg et al.*, 2011; *Staal et al.*, 2007]. As Fe may limit N_2 fixation [*Mills et al.*, 2004], here Fe inputs have been suggested to determine the large scale distribution of diazotrophs [*Moore et al.*, 2009]. We have now shown that although Aeolian dust transport from the Saharan/Sahel desert regions is considered the dominant external input of iron to the surface waters of the eastern (sub-) tropical North Atlantic Ocean, it can be exceeded by other DFe sources in our study region. Offshore advective transport from African continental shelf waters formed an important input of DFe to the open ocean in the northern part of our study area. In addition, vertical diffusive mixing formed an important source of DFe to the surface ocean where enhanced concentrations of DFe existed below the wind mixed layer, e.g., as generally in OMZs. In the south of our study area in the OMZ, vertical diffusive mixing as a source of DFe was equal to or even surpassed that of a major dust event. As the maintenance of OMZs may depend on N_2 fixation driven export [*Moore and Doney*, 2007] a feedback loop may exist where Fe from below forms a significant contribution to N_2 fixation driven export enhancing remineralization and strengthening the OMZ.

[35] **Acknowledgments.** We want to express our gratitude to the Master and crew of RRS *Discovery* for support during the cruise. We further want to thank Peter Statham and Alex Xylouri for all their help with sampling of the trace metals and Brian Dickie for his help with the measurement of DAl. Excellent support for the trace metal clean casts and shipboard underway measurements was provided by Chris Barnard, Allen Davies, John Wynar and John Short of NMF-SS. Furthermore, we want to thank Mark Stinchcombe for handling the logistics of the cruise and for measuring silicate. We thank Loes Gerringa for comments and advice. This research is funded by NERC as part of the UKSOLAS program, project grant NE/C001931/1.

References

Achterberg, E. P., T. W. Holland, A. R. Bowie, R. F. C. Mantoura, and P. J. Worsfold (2001), Determination of iron in seawater, *Anal. Chim. Acta*, *442*(1), 1–14, doi:10.1016/S0003-2670(01)01091-1.

Anderson, L. A. (1995), On the hydrogen and oxygen content of marine phytoplankton, *Deep Sea Res., Part I*, *42*(9), 1675–1680, doi:10.1016/0967-0637(95)00072-E.

Ardelan, M. V., O. Holm-Hansen, C. D. Hewes, C. S. Reiss, N. S. Silva, H. Dulaiova, E. Steinnes, and E. Sakshaug (2010), Natural iron enrichment around the Antarctic Peninsula in the Southern Ocean, *Biogeosciences*, *7*(1), 11–25, doi:10.5194/bg-7-11-2010.

Arimoto, R., and R. A. Duce (1986), Dry deposition models and the air sea exchange of trace elements, *J. Geophys. Res.*, *91*(D2), 2787–2792, doi:10.1029/JD091iD02p02787.

Baker, A. R., and P. L. Croot (2010), Atmospheric and marine controls on aerosol iron solubility in seawater, *Mar. Chem.*, *120*(1–4), 4–13, doi:10.1016/j.marchem.2008.09.003.

Baker, A. R., T. D. Jickells, K. F. Biswas, K. Weston, and M. French (2006), Nutrients in atmospheric aerosol particles along the Atlantic Meridional Transect, *Deep Sea Res., Part II*, *53*(14–16), 1706–1719, doi:10.1016/j.dsr2.2006.05.012.

Bartoli, G., C. Migon, and R. Losno (2005), Atmospheric input of dissolved inorganic phosphorus and silicon to the coastal northwestern Mediterranean Sea: Fluxes, variability and possible impact on phytoplankton dynamics, *Deep Sea Res., Part I*, *52*(11), 2005–2016, doi:10.1016/j.dsr.2005.06.006.

Bergquist, B. A., and E. A. Boyle (2006), Dissolved iron in the tropical and subtropical Atlantic Ocean, *Global Biogeochem. Cycles*, *20*, GB1015, doi:10.1029/2005GB002505.

Berman-Frank, I., J. T. Cullen, Y. Shaked, R. M. Sherrell, and P. G. Falkowski (2001), Iron availability, cellular iron quotas, and nitrogen fixation in Trichodesmium, *Limnol. Oceanogr.*, *46*(6), 1249–1260, doi:10.4319/lo.2001.46.6.1249.

Blain, S., G. Sarthou, and P. Laan (2008), Distribution of dissolved iron during the natural iron-fertilization experiment KEOPS (Kerguelen Plateau, Southern Ocean), *Deep Sea Res., Part II*, *55*(5–7), 594–605, doi:10.1016/j.dsr2.2007.12.028.

Bowie, A. R., E. P. Achterberg, P. L. Croot, H. J. W. de Baar, P. Laan, J. W. Moffett, S. Ussher, and P. J. Worsfold (2006), A community-wide intercomparison exercise for the determination of dissolved iron in seawater, *Mar. Chem.*, *98*(1), 81–99, doi:10.1016/j.marchem.2005.07.002.

Boyd, P. W., et al. (2005), FeCycle: Attempting an iron biogeochemical budget from a mesoscale SF6 tracer experiment in unperturbed low iron waters, *Global Biogeochem. Cycles*, *19*, GB4S20, doi:10.1029/2005GB002494.

Boyd, P. W., et al. (2007), Mesoscale iron enrichment experiments 1993–2005: Synthesis and future directions, *Science*, *315*(5812), 612–617, doi:10.1126/science.1131669.

Boyd, P. W., E. Ibisanmi, S. G. Sander, K. A. Hunter, and G. A. Jackson (2010), Remineralization of upper ocean particles: Implications for iron biogeochemistry, *Limnol. Oceanogr.*, *55*(3), 1271–1288, doi:10.4319/lo.2010.55.3.1271.

Brown, M. T., and K. W. Bruland (2008), An improved flow-injection analysis method for the determination of dissolved aluminum in seawater, *Limnol. Oceanogr. Methods*, *6*, 87–95, doi:10.4319/lom.2008.6.87.

Bucciarelli, E., S. Blain, and P. Treguer (2001), Iron and manganese in the wake of the Kerguelen Islands (Southern Ocean), *Mar. Chem.*, *73*(1), 21–36, doi:10.1016/S0304-4203(00)00070-0.

Charette, M. A., M. E. Gonneea, P. J. Morris, P. Statham, G. Fones, H. Planquette, I. Salter, and A. N. Garabato (2007), Radium isotopes as tracers of iron sources fueling a Southern Ocean phytoplankton bloom, *Deep Sea Res., Part II*, *54*(18–20), 1989–1998, doi:10.1016/j.dsr2.2007.06.003.

Chiapello, I., G. Bergametti, L. Gomes, B. Chatenet, F. Dulac, J. Pimenta, and E. S. Suares (1995), An additional low layer transport of Sahelian and Saharan dust over the north-eastern tropical Atlantic, *Geophys. Res. Lett.*, *22*(23), 3191–3194, doi:10.1029/95GL03313.

Dall'Osto, M., R. M. Harrison, E. J. Highwood, C. O'Dowd, D. Ceburnis, X. Querol, and E. P. Achterberg (2010), Variation of the mixing state

of Saharan dust particles with atmospheric transport, *Atmos. Environ.*, *44*(26), 3135–3146, doi:10.1016/j.atmosenv.2010.05.030.

de Baar, H. J. W., A. G. J. Buma, R. F. Nolting, G. C. Cadee, G. Jacques, and P. J. Treguer (1990), On iron limitation of the Southern Ocean: Experimental observation in the Weddell and Scotia Seas, *Mar. Ecol. Prog. Ser.*, *65*(2), 105–122, doi:10.3354/meps065105.

de Baar, H. J. W., et al. (2008), Titan: A new facility for ultraclean sampling of trace elements and isotopes in the deep oceans in the international Geotraces program, *Mar. Chem.*, *111*(1–2), 4–21, doi:10.1016/j.marchem.2007.07.009.

de Jong, J. T. M., J. den Das, U. Bathmann, M. H. C. Stoll, G. Kattner, R. F. Nolting, and H. J. W. de Baar (1998), Dissolved iron at subnanomolar levels in the Southern Ocean as determined by ship-board analysis, *Anal. Chim. Acta*, *377*(2–3), 113–124, doi:10.1016/S0003-2670(98)00427-9.

de Jong, J. T. M., M. Boye, M. D. Gelado-Caballero, K. R. Timmermans, M. J. W. Veldhuis, R. F. Nolting, C. M. G. van den Berg, and H. J. W. de Baar (2007), Inputs of iron, manganese and aluminium to surface waters of the Northeast Atlantic Ocean and the European continental shelf, *Mar. Chem.*, *107*, 120–142, doi:10.1016/j.marchem.2007.05.007.

Dillon, T. M. (1982), Vertical overturns: A comparison of Thorpe and Ozmidov length scales, *J. Geophys. Res.*, *87*, 9601–9613, doi:10.1029/JC087iC12p09601.

Duce, R. A., et al. (1991), The atmospheric input of trace species to the world ocean, *Global Biogeochem. Cycles*, *5*(3), 193–259, doi:10.1029/91GB01778.

Elrod, V. A., W. M. Berelson, K. H. Coale, and K. S. Johnson (2004), The flux of iron from continental shelf sediments: A missing source for global budgets, *Geophys. Res. Lett.*, *31*, L12307, doi:10.1029/2004GL020216.

Fofonoff, N. P., and R. C. Millard (1983), Algorithms for computation of fundamental properties of seawater, *UNESCO Tech. Pap. Mar. Sci.*, *44*, U.S. Educ., Sci. and Cult. Organ., Paris.

Galbraith, P. S., and D. E. Kelley (1996), Identifying overturns in CTD profiles, *J. Atmos. Oceanic Technol.*, *13*(3), 688–702, doi:10.1175/1520-0426(1996)013<0688:IOICP>2.0.CO;2.

Ganzeveld, L., J. Lelieveld, and G. J. Roelofs (1998), A dry deposition parameterization for sulfur oxides in a chemistry and general circulation model, *J. Geophys. Res.*, *103*(D5), 5679–5694, doi:10.1029/97JD03077.

Gerringa, L. J. A., A.-C. Alderkamp, P. Laan, C.-E. Thuróczy, H. J. W. de Baar, M. M. Mills, G. L. van Dijken, H. van Haren, and K. R. Arrigo (2012), Iron from melting glaciers fuels the phytoplankton blooms in Amundsen Sea (Southern Ocean): Iron biogeochemistry, *Deep Sea Res., Part II*, *71–76*, 16–31, doi:10.1016/j.dsr2.2012.03.007.

Gledhill, M., and C. M. G. van den Berg (1994), Determination of complexation of iron(III) with natural organic complexing ligands in seawater using cathodic stripping voltammetry, *Mar. Chem.*, *47*(1), 41–54, doi:10.1016/0304-4203(94)90012-4.

Hassler, C. S., and V. Schoemann (2009), Bioavailability of organically bound Fe to model phytoplankton of the Southern Ocean, *Biogeosciences*, *6*(10), 2281–2296, doi:10.5194/bg-6-2281-2009.

Hill, P. G., M. V. Zubkov, and D. A. Purdie (2010), Differential responses of Prochlorococcus and SAR11-dominated bacterioplankton groups to atmospheric dust inputs in the tropical Northeast Atlantic Ocean, *FEMS Microbiol. Lett.*, *306*(1), 82–89, doi:10.1111/j.1574-6968.2010.01940.x.

Hopkinson, B. M., and K. A. Barbeau (2007), Organic and redox speciation of iron in the eastern tropical North Pacific suboxic zone, *Mar. Chem.*, *106*, 2–17, doi:10.1016/j.marchem.2006.02.008.

Hosegood, P., H. van Haren, and C. Veth (2005), Mixing within the interior of the Faeroe-Shetland Channel, *J. Mar. Res.*, *63*(3), 529–561, doi:10.1357/0022240054307902.

Jickells, T. D., et al. (2005), Global iron connections between desert dust, ocean biogeochemistry, and climate, *Science*, *308*(5718), 67–71, doi:10.1126/science.1105959.

Johnson, K. S., R. M. Gordon, and K. H. Coale (1997), What controls dissolved iron concentrations in the world ocean?, *Mar. Chem.*, *57*(3–4), 137–161, doi:10.1016/S0304-4203(97)00043-1.

Karstensen, J., L. Stramma, and M. Visbeck (2008), Oxygen minimum zones in the eastern tropical Atlantic and Pacific oceans, *Prog. Oceanogr.*, *77*(4), 331–350, doi:10.1016/j.pocean.2007.05.009.

Kirkwood, D. (1996), Nutrients: Practical notes on their determination in sea water, *ICES Tech. in Mar. Environ. Sci., 17*, Int. Counc. for the Explor. of the Sea, Copenhagen.

Klunder, M. B., P. Laan, R. Middag, H. J. W. De Baar, and J. V. Ooijen (2011), Dissolved iron in the Southern Ocean (Atlantic sector), *Deep Sea Res.*, *58*, 2678–2694, doi:10.1016/j.dsr2.2010.10.042.

Kuma, K., J. Nishioka, and K. Matsunaga (1996), Controls on iron(III) hydroxide solubility in seawater: The influence of pH and natural organic chelators, *Limnol. Oceanogr.*, *41*(3), 396–407, doi:10.4319/lo.1996.41.3.0396.

Laës, A., S. Blain, P. Laan, E. P. Achterberg, G. Sarthou, and H. J. W. de Baar (2003), Deep dissolved iron profiles in the eastern North Atlantic in relation to water masses, *Geophys. Res. Lett.*, *30*(17), 1902, doi:10.1029/2003GL017902.

Lam, P. J., J. K. B. Bishop, C. C. Henning, M. A. Marcus, G. A. Waychunas, and I. Y. Fung (2006), Wintertime phytoplankton bloom in the subarctic Pacific supported by continental margin iron, *Global Biogeochem. Cycles*, *20*, GB1006, doi:10.1029/2005GB002557.

Landing, W. M., and K. W. Bruland (1987), The contrasting biogeochemistry of iron and manganese in the Pacific Ocean, *Geochim. Cosmochim. Acta*, *51*(1), 29–43, doi:10.1016/0016-7037(87)90004-4.

Landing, W. M., C. Haraldsson, and N. Paxeus (1986), Vinyl polymer agglomerate based transition-metal cation chelating ion-exchange resin containing the 8-hydroxyquinoline functional-group, *Anal. Chem.*, *58*(14), 3031–3035, doi:10.1021/ac00127a029.

Langlois, R. J., D. Hummer, and J. LaRoche (2008), Abundances and distributions of the dominant *nifH* phylotypes in the northern Atlantic Ocean, *Appl. Environ. Microbiol.*, *74*(6), 1922–1931, doi:10.1128/AEM.01720-07.

Law, C. S., E. R. Abraham, A. J. Watson, and M. I. Liddicoat (2003), Vertical eddy diffusion and nutrient supply to the surface mixed layer of the Antarctic Circumpolar Current, *J. Geophys. Res.*, *108*(C8), 3272, doi:10.1029/2002JC001604.

Liu, X. W., and F. J. Millero (2002), The solubility of iron in seawater, *Mar. Chem.*, *77*(1), 43–54, doi:10.1016/S0304-4203(01)00074-3.

Machín, F., and J. L. Pelegri (2009), Northward penetration of Antarctic Intermediate Water off northwest Africa, *J. Phys. Oceanogr.*, *39*(3), 512–535, doi:10.1175/2008JPO3825.1.

Mahowald, N., et al. (2008), Global distribution of atmospheric phosphorus sources, concentrations and deposition rates, and anthropogenic impacts, *Global Biogeochem. Cycles*, *22*, GB4026, doi:10.1029/2008GB003240.

Maldonado, M. T., R. F. Strzepek, S. Sander, and P. W. Boyd (2005), Acquisition of iron bound to strong organic complexes, with different Fe binding groups and photochemical reactivities, by plankton communities in Fe-limited subantarctic waters, *Global Biogeochem. Cycles*, *19*, GB4S23, doi:10.1029/2005GB002481.

Martin, J. H., and S. E. Fitzwater (1988), Iron-deficiency limits phytoplankton growth in the northeast Pacific Subarctic, *Nature*, *331*(6154), 341–343, doi:10.1038/331341a0.

Measures, C. I., and S. Vink (2000), On the use of dissolved aluminum in surface waters to estimate dust deposition to the ocean, *Global Biogeochem. Cycles*, *14*(1), 317–327, doi:10.1029/1999GB001188.

Measures, C. I., W. M. Landing, M. T. Brown, and C. S. Buck (2008), High-resolution Al and Fe data from the Atlantic Ocean CLIVAR-CO_2 repeat hydrography A16N transect: Extensive linkages between atmospheric dust and upper ocean geochemistry, *Global Biogeochem. Cycles*, *22*, GB1005, doi:10.1029/2007GB003042.

Mills, M. M., C. Ridame, M. Davey, J. La Roche, and R. J. Geider (2004), Iron and phosphorus co-limit nitrogen fixation in the eastern tropical North Atlantic, *Nature*, *429*(6989), 292–294, doi:10.1038/nature02550.

Moore, C. M., et al. (2009), Large-scale distribution of Atlantic nitrogen fixation controlled by iron availability, *Nat. Geosci.*, *2*(12), 867–871, doi:10.1038/ngeo667.

Moore, J. K., and S. C. Doney (2007), Iron availability limits the ocean nitrogen inventory stabilizing feedbacks between marine denitrification and nitrogen fixation, *Global Biogeochem. Cycles*, *21*, GB2001, doi:10.1029/2006GB002762.

Moore, W. S. (2000), Determining coastal mixing rates using radium isotopes, *Cont. Shelf Res.*, *20*(15), 1993–2007, doi:10.1016/S0278-4343(00)00054-6.

Neuer, S., T. Freudenthal, R. Davenport, O. Llinas, and M. J. Rueda (2002), Seasonality of surface water properties and particle flux along a productivity gradient off NW Africa, *Deep Sea Res., Part II*, *49*(17), 3561–3576, doi:10.1016/S0967-0645(02)00098-X.

Nishioka, J., et al. (2007), Iron supply to the western subarctic Pacific: Importance of iron export from the Sea of Okhotsk, *J. Geophys. Res.*, *112*, C10012, doi:10.1029/2006JC004055.

Obata, H., H. Karatani, and E. Nakayama (1993), Automated-determination of iron in seawater by chelating resin concentration and chemiluminescence detection, *Anal. Chem.*, *65*(11), 1524–1528, doi:10.1021/ac00059a007.

Okubo, A. (1971), Oceanic diffusion diagrams, *Deep Sea Res.*, *18*(8), 789–802, doi:10.1016/0011-7471(71)90046-5.

Patey, M. D., M. J. A. Rijkenberg, P. J. Statham, M. C. Stinchcombe, E. P. Achterberg, and M. Mowlem (2008), Determination of nitrate and phosphate in seawater at nanomolar concentrations, *TrAC Trends Anal. Chem.*, *27*(2), 169–182, doi:10.1016/j.trac.2007.12.006.

Planquette, H., et al. (2007), Dissolved iron in the vicinity of the Crozet Islands, Southern Ocean, *Deep Sea Res., Part II*, *54*(18–20), 1999–2019, doi:10.1016/j.dsr2.2007.06.019.

Powell, C. F. (2011), Atmospheric inputs of iron and other key nutrients to the tropical North Atlantic, PhD thesis, Univ. of East Anglia, Norwich, U. K.

Rijkenberg, M. J. A., L. J. A. Gerringa, K. R. Timmermans, A. C. Fischer, K. J. Kroon, A. G. J. Buma, B. T. Wolterbeek, and H. J. W. de Baar (2008a), Enhancement of the reactive iron pool by marine diatoms, *Mar. Chem.*, *109*(1–2), 29–44, doi:10.1016/j.marchem.2007.12.001.

Rijkenberg, M. J. A., C. F. Powell, M. Dall'Osto, M. C. Nielsdottir, M. D. Patey, P. G. Hill, A. R. Baker, T. D. Jickells, R. M. Harrison, and E. P. Achterberg (2008b), Changes in iron speciation following a Saharan dust event in the tropical North Atlantic Ocean, *Mar. Chem.*, *110*(1–2), 56–67, doi:10.1016/j.marchem.2008.02.006.

Rijkenberg, M. J. A., R. J. Langlois, M. M. Mills, M. D. Patey, P. G. Hill, M. C. Nielsdóttir, T. J. Compton, J. LaRoche, and E. P. Achterberg (2011), Environmental forcing of nitrogen fixation in the eastern tropical and sub-tropical North Atlantic Ocean, *PLoS ONE*, *6*(12), e28989, doi:10.1371/journal.pone.0028989.

Santana-Casiano, J. M., M. Gonzaalez-Davila, and F. J. Millero (2005), Oxidation of nanomolar levels of Fe(II) with oxygen in natural waters, *Environ. Sci. Technol.*, *39*(7), 2073–2079, doi:10.1021/es049748y.

Sarthou, G., et al. (2003), Atmospheric iron deposition and sea-surface dissolved iron concentrations in the eastern Atlantic Ocean, *Deep Sea Res., Part I*, *50*(10–11), 1339–1352, doi:10.1016/S0967-0637(03)00126-2.

Sarthou, G., A. R. Baker, J. Kramer, P. Laan, A. Laës, S. Ussher, E. P. Achterberg, H. J. W. de Baar, K. R. Timmermans, and S. Blain (2007), Influence of atmospheric inputs on the iron distribution in the subtropical north-east Atlantic Ocean, *Mar. Chem.*, *104*, 186–202, doi:10.1016/j.marchem.2006.11.004.

Staal, M., S. T. Hekkert, G. J. Brummer, M. Veldhuis, C. Sikkens, S. Persijn, and L. J. Stal (2007), Nitrogen fixation along a north-south transect in the eastern Atlantic Ocean, *Limnol. Oceanogr.*, *52*(4), 1305–1316, doi:10.4319/lo.2007.52.4.1305.

Stramma, L., and F. Schott (1999), The mean flow field of the tropical Atlantic Ocean, *Deep Sea Res., Part II*, *46*(1–2), 279–303, doi:10.1016/S0967-0645(98)00109-X.

Stramma, L., S. Huttl, and J. Schafstall (2005), Water masses and currents in the upper tropical northeast Atlantic off northwest Africa, *J. Geophys. Res.*, *110*, C12006, doi:10.1029/2005JC002939.

Stramma, L., P. Brandt, J. Schafstall, F. Schott, J. Fischer, and A. Körtzinger (2008), Oxygen minimum zone in the North Atlantic south and east of the Cape Verde Islands, *J. Geophys. Res.*, *113*, C04014, doi:10.1029/2007JC004369.

Sunda, W. G. (1997), Control of dissolved iron concentrations in the world ocean: A comment, *Mar. Chem.*, *57*(3–4), 169–172, doi:10.1016/S0304-4203(97)00045-5.

Thorpe, S. A. (1977), Turbulence and mixing in a Scottish loch, *Philos. Trans. R. Soc. London, Ser. A*, *286*(1334), 125–181, doi:10.1098/rsta.1977.0112.

Thuróczy, C. E., L. J. A. Gerringa, M. B. Klunder, R. Middag, P. Laan, K. R. Timmermans, and H. J. W. de Baar (2010), Speciation of Fe in the eastern North Atlantic Ocean, *Deep Sea Res., Part I*, *57*(11), 1444–1453, doi:10.1016/j.dsr.2010.08.004.

Tsuchiya, M., L. D. Talley, and M. S. McCartney (1992), An eastern Atlantic section from Iceland southward across the equator, *Deep Sea Res.*, *39*(11–12), 1885–1917.

Ussher, S. J., E. P. Achterberg, G. Sarthou, P. Laan, H. J. W. de Baar, and P. J. Worsfold (2010), Distribution of size fractionated dissolved iron in the Canary Basin, *Mar. Environ. Res.*, *70*(1), 46–55, doi:10.1016/j.marenvres.2010.03.001.

Voss, M., P. Croot, K. Lochte, M. Mills, and I. Peeken (2004), Patterns of nitrogen fixation along 10°N in the tropical Atlantic, *Geophys. Res. Lett.*, *31*, L23S09, doi:10.1029/2004GL020127.

Wagener, T., E. Pulido-Villena, and C. Guieu (2008), Dust iron dissolution in seawater: Results from a one-year time-series in the Mediterranean Sea, *Geophys. Res. Lett.*, *35*, L16601, doi:10.1029/2008GL034581.

Witter, A. E., B. L. Lewis, and G. W. Luther (2000), Iron speciation in the Arabian Sea, *Deep Sea Res., Part II*, *47*(7–8), 1517–1539, doi:10.1016/S0967-0645(99)00152-6.

Wooster, W. S., A. Bakun, and D. R. McLain (1976), Seasonal upwelling cycle along eastern boundary of North Atlantic, *J. Mar. Res.*, *34*(2), 131–141.

Wu, J. F., and G. W. Luther (1994), Size-fractionated iron concentrations in the water column of the western North Atlantic Ocean, *Limnol. Oceanogr.*, *39*(5), 1119–1129, doi:10.4319/lo.1994.39.5.1119.

Ye, Y., C. Volker, and D. A. Wolf-Gladrow (2009), A model of Fe speciation and biogeochemistry at the Tropical Eastern North Atlantic Time-Series Observatory site, *Biogeosciences*, *6*(10), 2041–2061, doi:10.5194/bg-6-2041-2009.